REPORT DOCUMENTATION PAGE

Form Approved
OMB No. 0704-0188

1. REPORT DATE *(DD-MM-YYYY)*	**2. REPORT TYPE**	**3. DATES COVERED** *(From - To)*
18-10-2005	Technical Paper	

4. TITLE AND SUBTITLE

Enhancement of Chamber Wall Heat Transfer by Surface Contouring (POSTPRINT)

5a. CONTRACT NUMBER
FA9300-04-C-0016

5b. GRANT NUMBER

5c. PROGRAM ELEMENT NUMBER

6. AUTHOR(S)
E. Coy, S. Danczyk, and J. Watts (AFRL/PRSA), J. Poylio (Northrop Grumman)

5d. PROJECT NUMBER
5026

5e. TASK NUMBER
0548

5f. WORK UNIT NUMBER

7. PERFORMING ORGANIZATION NAME(S) AND ADDRESS(ES)

Northrop Grumman Space & Missile Systems Corp.
Space Technology
One Space Park
Redondo Beach, CA 90278

8. PERFORMING ORGANIZATION REPORT NUMBER

AFRL-PR-ED-TP-2005-382

9. SPONSORING / MONITORING AGENCY NAME(S) AND ADDRESS(ES)

Air Force Research Laboratory (AFMC)
AFRL/PRS
5 Pollux Drive
Edwards AFB CA 93524-70448

10. SPONSOR/MONITOR'S ACRONYM(S)

11. SPONSOR/MONITOR'S NUMBER(S)
AFRL-PR-ED-TP-2005-382

12. DISTRIBUTION / AVAILABILITY STATEMENT

Approved for public release; distribution unlimited. PA number AFRL-ERS-PAS-05-247.

13. SUPPLEMENTARY NOTES
Presented at the 53rd JANNAF Joint Propulsion Meeting (JPM), 2nd Liquid Propulsion Subcommittee (LPS) and Spacecraft Propulsion Subcommittee (SPS), Monterey, CA, 5-8 Dec 2005.

14. ABSTRACT

The effect of surface features on chamber wall heat transfer has been measured in a sub-scale combustion chamber. Results are reported for five different roughness patterns for conditions of hydrogen/oxygen combustion at mixture ratios of 2-6 and chamber pressures of 100-200 psig. The results include the measured levels of heat flux and Stanton number. The transverse ribs and grooves had the largest effect, resulting in approximately a doubling of the heat flux relative to a smooth plate, and the increase in Stanton number agreed well with a correlation based on skin-friction.

15. SUBJECT TERMS

16. SECURITY CLASSIFICATION OF:			**17. LIMITATION OF ABSTRACT**	**18. NUMBER OF PAGES**	**19a. NAME OF RESPONSIBLE PERSON**
					Dr. Edward B. Coy
a. REPORT	**b. ABSTRACT**	**c. THIS PAGE**	A	13	**19b. TELEPHONE NUMBER** *(include area code)*
Unclassified	**Unclassified**	**Unclassified**			(661) 275-5219

ENHANCEMENT OF CHAMBER WALL HEAT TRANSFER BY SURFACE CONTOURING

E. Coy, S. Danczyk, J. Watts
Air Force Research Laboratory
Edwards AFB, CA

J. Poylio
Northrop Grumman Space Technology
Redondo Beach, CA

ABSTRACT

The effect of surface features on chamber wall heat transfer has been measured in a sub-scale combustion chamber. Results are reported for five different roughness patterns for conditions of hydrogen/oxygen combustion at mixture ratios of 2-6 and chamber pressures of 100-200 psig. The results include the measured levels of heat flux and Stanton number. The transverse ribs and grooves had the largest effect, resulting in approximately a doubling of the heat flux relative to a smooth plate and the increase in Stanton number agreed well with a correlation based on skin-friction.

INTRODUCTION

The Air Force Research Laboratory (AFRL), through the Integrated High Payoff Rocket Propulsion Technology Program (IHPRPT), has created the Upper Stage Engine Technology (USET) program. The goals of USET are to develop and validate modeling and simulation (M&S) tools that can be applied in the design of a high performing expander cycle engine operating on liquid oxygen and liquid hydrogen propellants. Hardware design, fabrication and testing performed under the program is primarily in support of the development and validation of M&S tools. The program is designed to provide risk reduction and increased effectiveness for any subsequent full-scale upper stage engine program.

A critical M&S need for the design of a high-performing expander cycle engine is chamber wall heat transfer prediction. Uncertainty in predictive methods results in large thermal design margins that have a significant impact on engine performance and thrust to weight ratio. The weakest link in existing models is the prediction of the hot-gas side conditions and convective heat transfer coefficient.

The chamber pressure that can be achieved in an expander cycle engine is largely determined by the amount of heat transferred through the chamber wall to the turbine drive gas. If the heat transfer is increased by lengthening the barrel section of the combustion chamber, the space envelope and weight of the engine are increased and the pressure drop in the cooling channels is increased. An alternative approach is to add heat transfer enhancement features to the chamber wall. This approach has been adopted in several development programs. Rocketdyne investigated the use of axial ribs to increase the heat transfer area in the Orbit Transfer Vehicle propulsion system trade studies performed for NASA and predicted that a 60% increase in heat transfer rate could be realized with 0.040 inch tall ribs[1,2]. Daimler Chrysler Aerospace (DASA) also examined the effects of ribs of various configurations and concluded that the increase in heat flux would be approximately equal to the increase in surface area[3].

Uncertainties in the heat transfer prediction are increased when features for enhancing heat flux are considered. AFRL in collaboration with Northrop Grumman Space Technology, has undertaken a test program to obtain chamber wall heat flux data for several types of

enhancement features using a sub-scale test article. The goal of this work is to produce data that can be used to validate heat transfer predictions using the analytical tools developed under USET.

EXPERIMENTAL SETUP

Tests were performed in the EC-1 laboratory located at the AFRL site at Edwards AFB, CA. The test rig is shown in Figure 1. The injector is a shear co-axial design with oxygen in the center and hydrogen in the surrounding annulus. Combustion reactions occur in the 2 inch square chamber. A vortex mixer was inserted to improve mixing across the cross-section. The entrance to the heat transfer rig is a 2 inch square to 1 inch square water-cooled transition. The rig is water-cooled and contains a 1 inch square channel for combustion gases. The test coupon forms the top of the channel and is a 6 inch long by 2 inch wide plate with the center 1 inch strip exposed to the hot gas. The gases exit through a choked, water-cooled, copper nozzle. The contraction ratio of the chamber from the test coupon location to the nozzle is 4.5. The overall L* is 177 inches. The square-channel design facilitates the testing of a wide variety of chamber wall coupons. The rig was originally designed by NGST for a chamber wall transpiration cooling study. It was adapted with minor modifications for the present work.

The test coupons were provided by NGST. Forty pounds of –325 mesh GRCop-84 powder were prepared by Crucible Research through a vacuum induction melting and inert gas atomization and screening process. The material was delivered to ASB Industries, Inc. for sample fabrication. The GRCop-84 was deposited to the required thickness (>0.200”) on smooth aluminum substrates by the cold spray process. After spraying, the substrate was machined away, and the remaining GRCop-84 was machined with the desired surface texture and to the desired thickness and surface finish (smoothness). No hot isostatic press (HIP) was done, because it would have provided very little, if any, benefit in terms of material density and thermal conductivity. Five coupons were produced. The dimensions of the surface features as well as post-test images are shown in Table 1. Calibrations of instrumentation were performed in-place using secondary calibration standards. The wiring and data acquisition channels were not changed between the calibrations and the tests. “Facility” data is omitted from this discussion.

Chamber pressures and system pressures were measured with Stellar Technology P/N ST-1500 pressure transducer, range 0-3000 psig, +/- 0.05% full scale, (+/- 1.5 psi). Calibrations were performed on 24 May 2005, 03 August 2005, and 17 August 2005 using a Ruska Model 7310 High Pressure Pneumatic Controller. The nominal accuracy of this device is 0.01% FS. The calibrations support the 0.05% uncertainty estimate.

Thermocouple accuracy was verified using a Neslab, EX-251HT high temperature bath containing ethylene glycol and varying the temperature over the range 70-250 F. The bath continuously re-circulates and contains an RTD sensor with a nominal accuracy of less than +/- 0.2 F. Based on this check, the thermocouples were assigned an uncertainty of +/- 3 F. No correction to the standard ASTM data for the TC types was necessary.

The intrinsic thermocouples mounted on the smooth GRCop-84 plate (discussed further below) were spot checked using an ice-bath, and a boiling water bath and showed agreement with the expected values within 1 C. The intrinsic thermocouples on the other plates were not checked against a temperature standard but the lead resistance was checked using an ohm-meter and the TCs were verified to be bonded to the plates. The intrinsic thermocouples were terminated at a reference junction oven from Pace Engineering Co. The temperature of the oven was stable to less than 0.1 C. Conduction errors on the thermocouple wires was assumed to be negligible as the thermal conductivity of the Type K thermocouple wire was an order of magnitude less than the GRCop-84 base material.

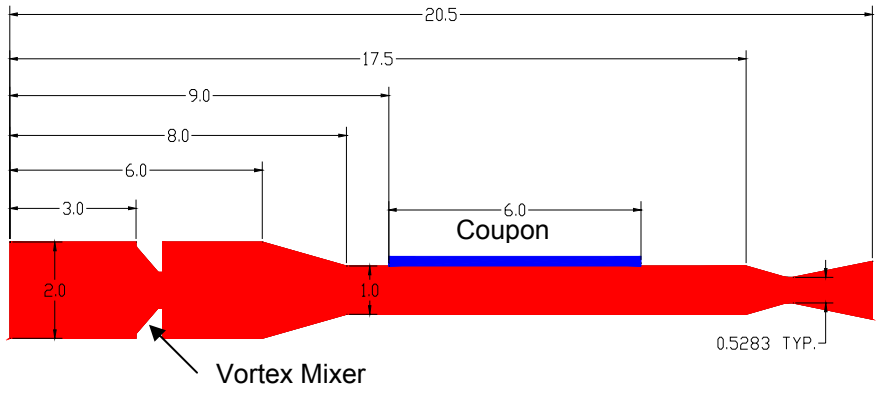

Figure 1. Heat transfer rig. Dimensions in inches.

Axial Ribs	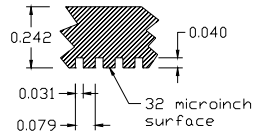	
Transverse Ribs	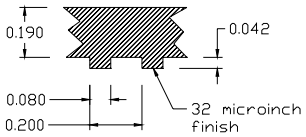	
Transverse Grooves	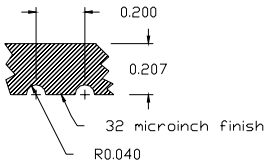	
Rough	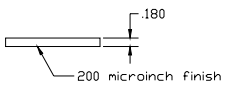	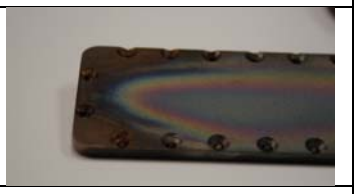
Smooth	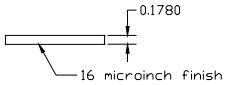	See Fig. 5

Table 1 GRCop-84 coupons with heat transfer enhancement features. Dimensions in inches.

Flow rates of gaseous oxygen and hydrogen were controlled and measured using sonic nozzles. Pressures and temperatures were measured upstream of the nozzles and pressures were measured downstream to ensure the nozzles were choked. The measured upstream values were taken to be equal to the stagnation values as the Mach number of the flow was less than 0.2. The nozzles were obtained from Flow-Dyne Engineering, Inc. The inlets were highly polished and contained a smooth radius at the throat. Discharge coefficients for the oxygen nozzles were measured in-place using a weigh tank and a timed flow of gaseous nitrogen. The calibration data supports an accuracy estimate of +/- 0.5%. The discharge coefficients were not measured for the hydrogen nozzles and a nominal Cd of 0.992 was used with an uncertainty estimate of +/-0.5%. The mass flow-rates were determined from the measured pressure, temperature and orifice diameter using a quasi-one-dimensional, isentropic approximation. The gas properties were obtained using the real-gas properties contained in the NIST REFPROP database. These are the most accurate properties available and the errors in properties were assumed to be negligible compared to other sources of error. During the firing sequence the gas upstream of the oxygen sonic nozzle underwent significant adiabatic compression which caused a temperature transient which persisted for up to 5 seconds after the fire valve opened. The time response of the thermocouple was not sufficient to resolve the temperature excursion. We have estimated the effect on accuracy at +/- 2%.

Uncertainty in flow rate was determined using the general rule for combining errors.

$$\sigma_{\dot{m}} = \left[\left(\frac{\partial \dot{m}}{\partial P} \right)^2 \sigma_P^2 + \left(\frac{\partial \dot{m}}{\partial T} \right) \sigma_T^2 + \left(\frac{\partial \dot{m}}{\partial C_D} \right) \sigma_{C_D}^2 \right]^{1/2}.$$

The errors in temperature, pressure and discharge coefficient were assumed to be uncorrelated. The uncertainty in the throat area was not explicitly included as it was implicitly included in the discharge coefficient uncertainty.

Chamber throat diameter was measured after each test to check for nozzle erosion. The throat was measured using a Starrett SPC-plus digital electronic internal micrometer with 3 point carbide contacts. The device reads to 0.0001 inch however, in practice the variability between operators is typically on the order 0.0005 inch. For the cases presented in this report, no nozzle erosion was detected. The nozzle is Alloy 101 (OFHC) and is water-cooled. Thermal expansion during the run and effects of pressure on the throat may cause dimensional changes from the cold condition on the order of 0.005 inch. The cold dimension is reported in the data set and used in the C* calculations. Given these considerations we have estimated the uncertainty in the throat area as +/- 2%.

*C** was calculated directly from the definition, $C^* = P_c A^* / (\dot{m}_{O_2} + \dot{m}_{H_2})$. The values for chamber pressure and mass flow were averages over a time window that was selected "by eye" after the run and was typically 0.5 to 1 second in length. The window was selected to begin after the initial ramping up of chamber pressure, end just before the closing of the firing valves, and to represent steady state operation. This somewhat subjective approach was adopted because the ramping up time depended on a number of factors relating to the sonic nozzles, the feed pressures, the injector, the target chamber pressure, the heat-sink chamber, and other factors and therefore it was not possible to adopt a single timing criterion that worked well in all cases. The run time was also adjusted as necessary to produce an appropriate length data window while keeping the maximum temperature of the plate below 800 F.

The combustion efficiency metric $\eta_{C^*}=C^*/C^*_{ideal}$ was calculated using a theoretical value of C^*_{ideal} obtained from the Gordon and McBride equilibrium code, CEA, and was not corrected for any losses due to heat transfer, boundary layers, kinetics, or mixing. The reported η_{C^*} values

are typically in the range of 0.85-0.93. The major source of loss was heat transfer. This was verified by installing an injector with very high mixing efficiency. No effect on η_{C^*} was observed indicating that the flow had been well mixed and likely completely reacted.

In the error calculation for η_{C^*}, the errors in C^* and C^*_{ideal} are not independent since $C^*_{ideal} = f(\dot{m}_{O_2}, \dot{m}_{H_2}, A^*)$ and both C^* and C^*_{ideal} depend on $\dot{m}_{O_2}$, $\dot{m}_{H_2}$ and A^*. In this case the sources of error can be treated as independent if the propagation of error equation is applied directly to the definition,

$$\eta_{C^*_{ideal}} = \frac{P_C A^* / (\dot{m}_{O_2} + \dot{m}_{H_2})}{C^*_{ideal}(\dot{m}_{O_2}, \dot{m}_{H_2}, A^*)}.$$

Due to the contoured surfaces of the plates, conventional heat flux instrumentation could not be used to measure heat flux to the surface directly. The heat flux was determined from backside temperature measurements using the following approach. The temperature in a finite thickness, infinite slab exposed to a constant heat flux at representative conditions initially rises faster on the side exposed to the heat flux, however, after approximately 1 second, both sides rise at the same rate and the rate of change of temperature is proportional to the heat flux. In the experimental configuration, heat can flow in three dimensions. An order of magnitude analysis showed that the most significant term was the transverse heat flux to the cold edges. To verify this result a complete model of the conduction problem was created using Fluent 6.1. A result is given in Figure 2. In this model the convection coefficient and bulk gas temperature were constant so the heat flux at the surface decreases as the surface temperature rises. Shown in the figure are three approximations to the surface heat flux derived from backside temperature measurements. All three have large errors during the initial period of the transient heating before the heat has diffused through the plate. The "lumped" approximation neglects the conduction along the plate and uses the approximation,

$$\dot{q}'' = \rho C_P l \frac{dT}{dt},$$

where l is the thickness of the plate. The remaining two approximations are based on the heat conduction equation,

$$\dot{q}'' = k l \left(\frac{1}{\alpha} \frac{\partial T}{\partial t} - \nabla^2 T \right)$$

where heat flux to the surface is treated as a source term in a two-dimensional geometry. The Laplacian term is obtained from finite difference approximations using temperatures measured on the backside of the plate. In Figure 2, the improvement due to the inclusion of the transverse heat flux is shown. Based on this analysis, a pattern of thermocouples on the backside was used that would allow a 2nd order approximation for the transverse heat flux. The pattern is shown by the location of the "Xs" in Figure 3.

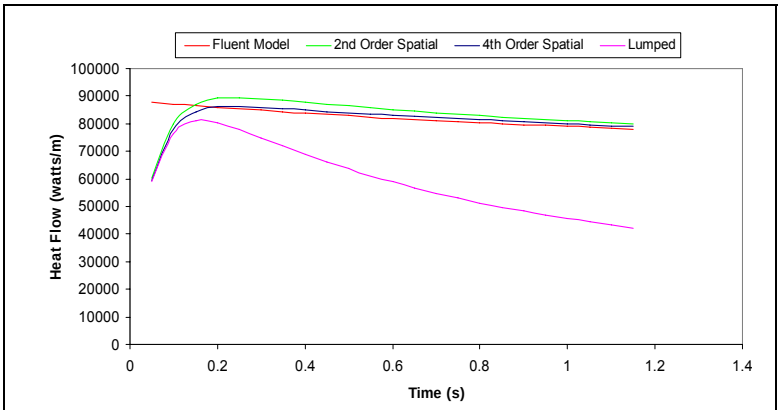

Figure 2. Simulation of transient heat flux to 3-D GRCop-84 plate using Fluent 6.1 and 3 approximations for determining the heat flux based only on backside surface temperature measurements.

The uncertainty in the heat flux measurement depends on the uncertainty in the measured temperatures as well as the properties of the material. The reference data used for the thermal properties was based on samples from bars formed by extrusion[4]. The GRCop-84 coupons used in this study were formed using the cold spray technique and no hot iso-static

press was applied to achieve densification or annealing of the microstructure. The effect of the manufacturing method on the properties was discussed with David Ellis, one of the studies original authors[5].

The cold sprayed material would have initially had considerable cold work and therefore high residual stresses and dislocation densities without a HIP or anneal cycle. Assuming at least a 50% deformation in the powder particles, a sample heated above 200C will anneal almost immediately (<<15 minutes). Therefore the annealed GRCop-84 is representative of most if not all of the samples tested. Based on this evaluation the properties given in NASA/CR-2000-210055 were used.

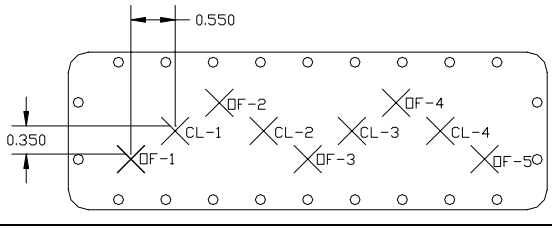

Figure 3 Pattern of thermocouples applied to backside of test coupons. Dimensions in inches.

The final form of the heat conduction equation used in data reduction was,

$$\dot{q}'' = k\, l \left(\frac{1}{\alpha} \dot{T}_{CL} - \frac{T_{OF_{-1}} - 2T_{CL} + T_{OF_{+1}}}{(\Delta y)^2} \right).$$

The reported heat flux is an average over the data window. For the centerline temperatures, the time rate of change term was evaluated by linear-regression over the data window and the temperatures in the Laplacian term were evaluated at the mid-point of the data window. The thermal properties were evaluated at the measured centerline temperature at the mid-point of the data window. The thickness of the plate was based on the mean values given in the following table.

Coupon	Average Thickness
Smooth	.178 in
Rough	.180 in.
Longitudinal Ribs	.229 in.
Transverse Ribs	.208 in.
Transverse Grooves	.194 in.

Table 2 Average thickness of coupon

The major source of error in the heat flux measurement is the transverse heat flux. Figure 4 shows the magnitude of the Laplacian term relative to the total heat flux delivered to the plate. As expected, the term is negative due to the diffusion of heat from the center of the plate to the cold edges, and the magnitude agrees well with the modeling predictions described above; however, there is a large amount of scatter that can not be readily explained or corrected. The variability may be due to real non-uniformities in the heat flux caused by hot-spots and streaking on the plate. Post-test inspections showed patterns consistent with flame attachment or impingement at varying locations along the plate. An example is shown in Fig. 5. The coarse grid of thermocouples used in this study was probably insufficient to resolve the gradients which existed in the plate.

There appears to be correlation between the plate type and the amount of scatter. The smooth plate and the plate with axial ribs exhibit larger scatter than the roughened plate and the plates with transverse patterns. The roughness elements may be providing a stabilizing effect on the flow and reducing the propensity towards streaking.

The best approach appears to be to eliminate the problem with a redesign rather than attempt to perform more detailed measurements that resolve the hot spots. It appears that a new injector is needed that will produce a uniformly mixed flow at the entrance to the test channel. We will also consider a new approach that will cause the heat transfer to be nearly one-dimensional and finely resolved spatially.

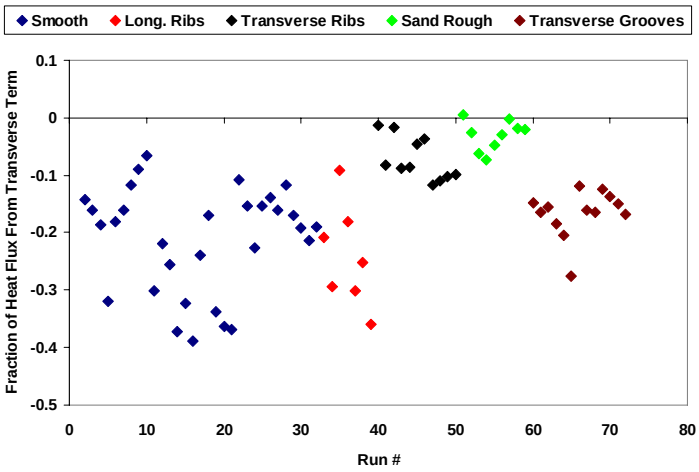

Figure 4. Plot of the relative magnitude of the transverse diffusion of heat in the plate relative to the total heat flux for all of the runs in the data set. Run # is an arbitrary index.

The other terms in the heat flux equation contribute relatively little to the uncertainty. The uncertainty in the linear fit to the unsteady centerline temperature is negligible. The uncertainties in the material properties were discussed above and are in the range of 2-5%. The uncertainty in the plate thickness term is also negligible. Given the difficulties associated with assigning an uncertainty to the transverse diffusion term, we have made an arbitrary estimate of +/- 15% for the overall heat flux.

The Stanton number is defined as,

$$St = \frac{q''_W}{\rho_\infty U_\infty (h_\infty - h_W)}.$$

It represents the fraction of the thermal energy available in the flow that is transferred to the wall on a per unit area basis.

The individual terms were evaluated as follows. The heat flux, q''_W, was discussed above. In the denominator, the term $\rho_\infty U_\infty$ is simply the mass flux which is obtained from the measured mass flow and channel area. The enthalpy of the flow, h_∞, was not measured directly and therefore was determined from an equilibrium calculation and corrected for heat loss using the measured value of η_{C^*} as follows. Based on the ideal, constant heat capacity ratio approximation for C^*,

$$\eta_{C^*} = \sqrt{T_0 / T_{0,ideal}}.$$

Making the approximation,

$$\sqrt{h_\infty / h_{\infty,ideal}} \approx \sqrt{T_0 / T_{0,ideal}},$$

we have,

$$h_\infty = h_{\infty,ideal}\, \eta^2_{C^*}.$$

Figure 5. Post-test image of smooth plate showing non-uniform heat marks.

The enthalpy of the fluid at the wall was determined using CEA assuming the flow was completely mixed. The enthalpy was evaluated at the chamber pressure and a wall temperature estimated using the following analytical approximation.

For the purposes of estimating surface temperature, we modeled the coupon as a uniform slab of a thickness *l* equal to the average thickness given in table 2 with constant thermal diffusivity, α , at an initially uniform temperature, *T(x,0)*. The backside of the slab, *x=0*, is adiabatic and at time, *t=0,* the front side, *x=l*, is suddenly exposed to a constant heat flux. The ratio of the temperatures on the two sides is given by the following expression based on eq.(5-33) of Arpaci, Conduction Heat Transfer, 1966,

$$\frac{T(l,t)-T(x,0)}{T(0,t)-T(x,0)} = \frac{Fo + 1/3 - 2\sum_{n=1}^{\infty} \frac{e^{-(n\pi)^2 Fo}}{(n\pi)^2}}{Fo - 1/6 - 2\sum_{n=1}^{\infty} \frac{(-1)^n e^{-(n\pi)^2 Fo}}{(n\pi)^2}}$$

where, $Fo = \alpha t / l^2$, is the Fourier number. The thermal diffusivity was evaluated at the backside temperature at the average temperature of the time interval.

The analytical model assumes that a step change in heat flux occurs at *t=0*. The time origin was defined as the point when chamber pressure had risen to half the average value in the data window. The value of *t* used to calculate *Fo* is the time elapsed between the origin and the midpoint of the data interval.

The temperatures and surface enthalpies derived in this way represent effective quantities. The actual surface temperature and enthalpy would be expected to vary with higher temperatures on the protruding parts of the contoured surface. This is an unavoidable consequence of using a Stanton number to correlate the data. The consequences it may have for inter-comparisons between smooth and contoured plates is not straightforward. In the future, when comparing with CFD results, the comparison will be made directly with the backside measurements through conjugate heat transfer modeling, avoiding the need for this approximation.

The uncertainty of the Stanton number is controlled by the uncertainty in the heat flux, discussed above, and the surface enthalpy, which depends on the surface temperature and the method used to convert this to an enthalpy. If we take the surface temperature uncertainty as +/- 50 F, the overall uncertainty is approximately +/- 16%.

RESULTS

The test matrix consisted of 3 mixture ratios (2,4,6), 2 chamber pressures (100, 200 psig), and the five coupons. Repeat tests were performed at several conditions and a total of 71 tests are included in the data set. A summary of the data is given in Table 3.

Typical results for heat flux are given in Figure 6. The addition of the transverse ribs resulted in a doubling of the heat flux for the three mixture ratios and two pressures. Figure 6 also shows heat flux measurements were very repeatable.

The results for Stanton number for the entire data set are given in Figure 7. The length scale used for the Reynolds number was the channel width and the fluid properties were based on the mean flow with accounting for heat loss. The data falls into two groups with the smooth, rough and axial rib coupons in the lower group. The axial ribs did not produce a significant increase in the Stanton number relative to the smooth plate. The spacing between the ribs may have been too small to allow circulation of the fluid. The rough plate Stanton number is the lowest of the group. This surprising result may be related to the smaller scatter in the transverse heat flux due to reduced streaking and hot spots as discussed above.

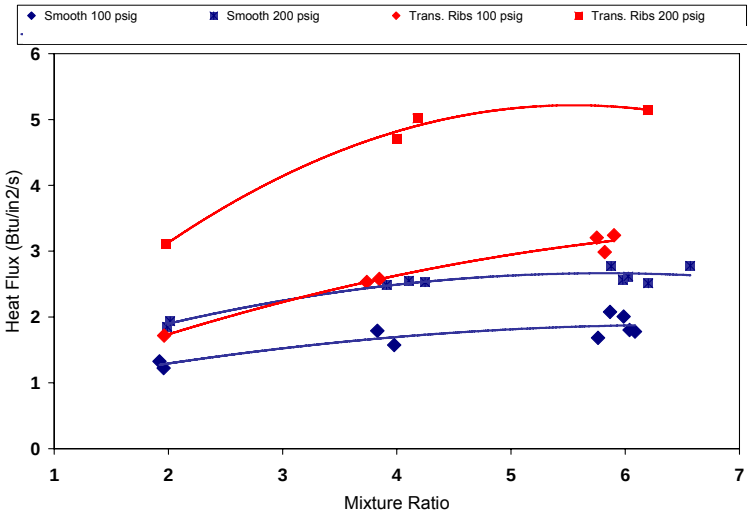

Figure 6 Heat flux results showing enhancement due to transverse ribs.

The transverse surface features resulted in nearly a doubling of the Stanton number relative to the smooth plate. The transverse ribs were somewhat more effective than the transverse grooves.

A correlation for Stanton number for a turbulent boundary layer on a smooth plate with negligible property variations is included in the figure[6]. This correlation assumes the momentum and thermal boundary layers are the same thickness and is valid for 0.5<Pr<1.0. The CEA predictions for Pr for the conditions of this study are in the range of 0.4-0.5.

$$St = 0.0287\ \mathrm{Re}_x^{-0.2}\ \mathrm{Pr}^{-0.4}.$$

The length scale used in the correlation is the distance from the leading edge of the plate. This was approximated as the distance from the start of the 1 inch channel to the midpoint of the coupon, or four inches. The difference in the length scales used to define *Re* was accounted for and the function actually plotted is,

$$St = 0.0208\ \mathrm{Re}^{-0.2}\ \mathrm{Pr}^{-0.4}.$$

The correlation overpredicts the measured Stanton number for the smooth plate by about 25%. This level of agreement is probably as good as one might expect given the approximations involved and the uncertainty in the experimental data. However, we can consider whether the difference could be reduced by improving the approximations.

One possible cause may be the variation in fluid properties across the boundary layer. Studies which have examined the effect of cooled walls on heat transfer are reviewed by Kays, Crawford and Weigand[7]. For temperature ratios up to 2, the effect can be correlated using a power law,

$$\frac{St}{St_{CP}} = \left(\frac{T_S}{T_\infty}\right)^n.$$

For turbulent flow in tubes the effect is small and the recommended value of n is zero.

Another cause could be the length scale used in the Reynolds number does not represent the actual state of development of the boundary layer. The virtual origin of the boundary layer may lie at a point upstream of the start of the 1 inch channel. To bring the correlation into the middle of the data scatter, the length scale in the Reynolds number would have to increase by approximately a factor of 4. Further work will be required in order to establish the significance of these results.

The effect of adding surface roughness can be accounted using a method suggested by Norris, and reviewed by Kays, et.al. (2005),

$$\frac{St}{St_{Smooth}} = \left(\frac{c_f}{c_{f\ Smooth}} \right)^n ,$$

where $n=0.68\ Pr^{0.215}$. When $c_f / c_{f\ smooth} > 4.0$ St no longer increases because the resistance to heat flow is controlled by the fluid trapped between the roughness elements. This correlation predicts that the heat flux for the transverse grooves will increase by a factor of 2. This is in agreement with the observed increase.

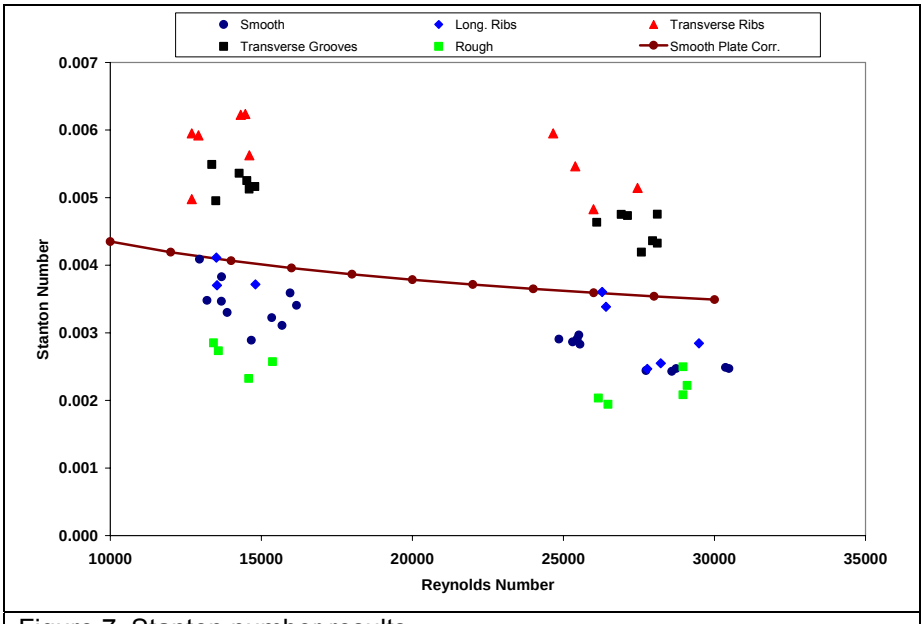

Figure 7 Stanton number results

CONCLUSION

Data on chamber wall heat flux under representative conditions is required for validation of software tools being developed under the USET program. In this paper we report on the first phase of this work which involved an investigation of the effects of surface contouring on heat transfer enhancement. The effects of specific contours on heat flux and Stanton number are reported. Future work will examine higher heat flux conditions. The first phase of this program identified a number of "lessons-learned" that will be factored into the upcoming tests.

Run #	Coupon	press. psig	u-press psi	O2/H2	u-O2/H2	etaCstar	u-etaCstar	q-Avg. Btu/in^2/s	u q-Avg. Btu/in^2/s	St-Avg.	u St-Avg.
Run85	Long. Rib	94.3	1.5	6.24	0.18	0.881	0.024	2.21	0.33	0.00372	0.00056
Run86	Long. Rib	97.3	1.5	3.99	0.11	0.871	0.024	2.09	0.31	0.00411	0.00062
Run87	Long. Rib	93.3	1.5	1.98	0.06	0.863	0.024	1.43	0.21	0.00370	0.00056
Run89	Long. Rib	191.1	1.5	6.43	0.18	0.894	0.022	2.92	0.44	0.00247	0.00037
Run90	Long. Rib	194.7	1.5	6.42	0.18	0.905	0.023	2.90	0.44	0.00255	0.00038
Run92	Long. Rib	202.9	1.5	6.53	0.18	0.922	0.023	3.30	0.50	0.00284	0.00043
Run93	Long. Rib	202.7	1.5	4.42	0.12	0.915	0.023	3.35	0.50	0.00339	0.00051
Run94	Long. Rib	198.3	1.5	2.20	0.06	0.903	0.023	2.76	0.41	0.00360	0.00054
Run102	Trans. Rib	95.5	1.5	5.82	0.16	0.893	0.025	2.99	0.45	0.00563	0.00084
Run104	Trans. Rib	93.9	1.5	5.90	0.17	0.883	0.024	3.24	0.49	0.00624	0.00094
Run111	Trans. Rib	93.8	1.5	5.75	0.16	0.889	0.025	3.20	0.48	0.00623	0.00093
Run112	Trans. Rib	91.4	1.5	3.74	0.11	0.870	0.024	2.53	0.38	0.00595	0.00089
Run113	Trans. Rib	92.9	1.5	3.85	0.11	0.864	0.024	2.58	0.39	0.00592	0.00089
Run114	Trans. Rib	93.4	1.5	1.96	0.06	0.869	0.024	1.72	0.26	0.00498	0.00075
Run107	Trans. Rib	191.6	1.5	6.20	0.18	0.899	0.022	5.14	0.77	0.00514	0.00077
Run108	Trans. Rib	189.9	1.5	4.18	0.12	0.878	0.022	5.02	0.75	0.00595	0.00089
Run109	Trans. Rib	197.4	1.5	4.00	0.11	0.866	0.022	4.71	0.71	0.00546	0.00082
Run110	Trans. Rib	191.6	1.5	1.98	0.06	0.880	0.022	3.11	0.47	0.00483	0.00073
Run116	Rough	95.4	1.5	5.81	0.16	0.885	0.024	1.34	0.20	0.00233	0.00035
Run117	Rough	99.0	1.5	6.18	0.17	0.910	0.025	1.50	0.23	0.00257	0.00039
Run118	Rough	96.3	1.5	4.05	0.11	0.879	0.024	1.37	0.21	0.00285	0.00043
Run119	Rough	93.2	1.5	1.94	0.05	0.859	0.024	0.97	0.15	0.00273	0.00041
Run120	Rough	198.5	1.5	6.56	0.19	0.928	0.023	2.25	0.34	0.00208	0.00031
Run121	Rough	209.0	1.5	5.83	0.16	0.921	0.023	2.40	0.36	0.00222	0.00033
Run122	Rough	199.1	1.5	4.13	0.12	0.902	0.023	2.27	0.34	0.00250	0.00037
Run123	Rough	196.4	1.5	2.15	0.06	0.896	0.023	1.46	0.22	0.00204	0.00031
Run124	Rough	197.2	1.5	2.06	0.06	0.899	0.023	1.38	0.21	0.00194	0.00029
Run130	Trans. Grv.	92.8	1.5	5.84	0.17	0.870	0.024	2.77	0.42	0.00536	0.00080
Run132	Trans. Grv.	95.8	1.5	5.77	0.16	0.879	0.024	2.72	0.41	0.00513	0.00077
Run133	Trans. Grv.	94.4	1.5	5.89	0.17	0.866	0.024	2.77	0.42	0.00525	0.00079
Run134	Trans. Grv.	97.0	1.5	5.82	0.16	0.889	0.024	2.77	0.41	0.00517	0.00077
Run135	Trans. Grv.	96.0	1.5	4.01	0.11	0.857	0.024	2.51	0.38	0.00549	0.00082
Run136	Trans. Grv.	92.7	1.5	1.94	0.05	0.845	0.024	1.70	0.26	0.00495	0.00074
Run137	Trans. Grv.	193.9	1.5	6.08	0.17	0.905	0.023	4.23	0.63	0.00419	0.00063
Run138	Trans. Grv.	198.1	1.5	5.98	0.17	0.907	0.023	4.43	0.66	0.00436	0.00065
Run139	Trans. Grv.	198.8	1.5	6.02	0.17	0.902	0.022	4.43	0.66	0.00433	0.00065
Run140	Trans. Grv.	201.3	1.5	3.88	0.11	0.887	0.022	4.14	0.62	0.00476	0.00071
Run141	Trans. Grv.	194.1	1.5	2.05	0.06	0.880	0.022	3.08	0.46	0.00464	0.00070
Run142	Trans. Grv.	211.1	1.5	4.12	0.12	0.887	0.022	4.37	0.66	0.00473	0.00071
Run143	Trans. Grv.	209.9	1.5	4.04	0.11	0.894	0.022	4.32	0.65	0.00475	0.00071
Run70	Smooth	94.5	1.5	6.05	0.17	0.896	0.025	1.57	0.24	0.00289	0.00043
Run71	Smooth	99.8	1.5	6.04	0.17	0.930	0.025	1.80	0.27	0.00322	0.00048
Run72	Smooth	94.8	1.5	3.98	0.11	0.900	0.025	1.58	0.24	0.00348	0.00052
Run74	Smooth	94.3	1.5	1.96	0.06	0.896	0.025	1.23	0.18	0.00347	0.00052
Run145	Smooth	90.2	1.5	5.76	0.16	0.852	0.024	1.69	0.25	0.00330	0.00050
Run157	Smooth	93.3	1.5	3.83	0.11	0.873	0.025	1.79	0.27	0.00409	0.00061
Run158	Smooth	93.9	1.5	1.92	0.05	0.852	0.024	1.33	0.20	0.00383	0.00057
Run146	Smooth	106.4	1.5	5.99	0.17	0.904	0.024	2.01	0.30	0.00341	0.00051
Run147	Smooth	105.6	1.5	5.87	0.17	0.899	0.024	2.08	0.31	0.00359	0.00054
Run149	Smooth	102.0	1.5	6.09	0.17	0.896	0.024	1.78	0.27	0.00311	0.00047
Run96	Smooth	210.0	1.5	6.57	0.19	0.927	0.023	2.78	0.42	0.00247	0.00037
Run97	Smooth	193.6	1.5	6.20	0.18	0.919	0.023	2.51	0.38	0.00244	0.00037
Run98	Smooth	191.1	1.5	4.25	0.12	0.905	0.023	2.53	0.38	0.00291	0.00044
Run99	Smooth	197.1	1.5	3.91	0.11	0.909	0.023	2.49	0.37	0.00287	0.00043

Run100	Smooth	188.4	1.5	1.99	0.06	0.904	0.023	1.85	0.28	0.00283	0.00043
Run150	Smooth	218.4	1.5	5.88	0.17	0.918	0.023	2.77	0.42	0.00249	0.00037
Run152	Smooth	203.1	1.5	5.98	0.17	0.917	0.023	2.57	0.38	0.00243	0.00036
Run153	Smooth	203.6	1.5	6.03	0.17	0.919	0.023	2.62	0.39	0.00247	0.00037
Run154	Smooth	197.2	1.5	4.10	0.12	0.904	0.023	2.55	0.38	0.00291	0.00044
Run155	Smooth	188.6	1.5	2.02	0.06	0.896	0.023	1.94	0.29	0.00297	0.00045

Table 3 Summary of run conditions, heat flux and average Stanton number. u denotes uncertainty.

[1] Baily, R.D., Defever, G.J., Wagner, W.R., “Enhanced Heat Transfer Rocket Combustor Technology,” JANNAF Propulsion Meeting, 1985, CPIA Pub. 425, Vol. IV, pp. 251-259

[2] Baily, R.D., “Enhanced Heat Transfer Rocket Technology,” JANNAF Propulsion Meeting, 1986, CPIA Pub. 455, Vol. IV, pp. 391-422

[3] Immich, H., Frohlich, T., Kretschmer, J., "Technology Developments for Expander Cycle Thrust Chambers", AIAA 99-2889, 35th JPC, Los Angeles, CA, 1999

[4] Ellis, D.L., Keller, D.J., "Thermophysical Properties of GRCop-84," NASA/CR-2000-210055, June 2000

[5] Private Communication

[6] Moffat, R.J., Kays, W.M., "A Review of Turbulent-Boundary-Layer Heat Transfer Research at Stanford 1958-1983", Advances in Heat Transfer, Vol. 16, 1984, pp. 241-365

[7] Kays, W., Crawford, M., Weighand, B., "Convective Heat and Mass Transfer, 4th ed.", McGraw Hill, 2005, p.341